


Forming a dielectric exciton phase in strongly correlated systems with spin crossover

Yu. S. Orlov,^{*} S. V. Nikolaev, V. A. Dudnikov[✉], and S. G. Ovchinnikov[✉]

*Institute of Engineering and Radio Electronics, Siberian Federal University, 660041 Krasnoyarsk, Russia
and Kirensky Institute of Physics, Federal Research Center KSC SB RAS, 660036 Krasnoyarsk, Russia*

 (Received 14 May 2021; revised 15 September 2021; accepted 12 October 2021; published 3 November 2021)

Formation of the magnetic structure and exciton condensate of local magnetic excitons in strongly correlated systems near the spin crossover under high pressure is considered in terms of the effective Hamiltonian obtained from a two-band Hubbard model in the regime of strong electron correlations. The coexistence of the long-range antiferromagnetic order and exciton condensate and the occurrence of the magnetization caused by the condensation of local magnetic excitons are demonstrated. Transformation of the electronic structure of the antiferromagnetic high-spin insulator into the paramagnetic two-band correlated metal via a narrow-gap antiferromagnetic excitonic semiconductor is obtained.

DOI: [10.1103/PhysRevB.104.195103](https://doi.org/10.1103/PhysRevB.104.195103)

I. INTRODUCTION

The formation and condensation of electron-hole pairs (excitons) in semimetals and semiconductors was predicted more than half a century ago [1,2]. The weak-coupling theory of the excitonic insulators has been developed analogously to the Bardeen-Cooper-Schrieffer (BCS) theory of superconductivity [3,4]. Later the ideas of excitonic condensation were discussed for strongly correlated materials within the Hubbard-type models. Recently in the review [5] of the different approaches to the excitonic condensation in Hubbard-type models the corresponding phase diagrams and connections to some other relevant models such as the Blume-Emery-Griffiths model [6] and bosonic t - J or bilayer Heisenberg [7] model have been discussed. Within the multiband Hubbard-type model the interrelation of the excitonic condensation and the high spin (HS)–low spin (LS) crossover takes place [8–14]. The minimal model which contains the multiorbital physics and excitonic effects is the two-band Hubbard-type model; different approaches to this model have been discussed in the review [5], in both the strong-coupling and weak-coupling regimes. In the strong-coupling limit we have suggested [15] an approach similar to Hubbard’s original one [16] that starts with the exact diagonalization of the local part of the Hamiltonian and construction of the Hubbard X operators. Within such approach the effective Hamiltonian has been obtained that was used to study the phase diagram and the HS-LS crossover under external pressure. The spin exciton interatomic hopping and excitonic condensation within this effective Hamiltonian as well as the change of the electronic structure due to spin crossover and excitonic condensation will be considered below. A spin gap between the LS and the HS is an external parameter of our model that may be varied by pressure. The mean-field phase diagram in the plane spin gap–temperature (which is equivalent to the diagram pressure–

temperature) contains the HS antiferromagnetic (HS-AFM) and paramagnetic (HS-PM), excitonic (Ex), and nonmagnetic LS ones. The excitonic phase appears in the spin crossover region and coexists with the HS AFM phase.

The rest of the paper is organized as follows. The two-band Hubbard-Kanamori model and its effective Hamiltonian in the strong-coupling regime are described in Sec. II. The phase diagrams for different parameter sets are discussed in Sec. III. The electronic structure for different phases is calculated in Sec. IV. Discussion of results is given in Sec. V.

II. EFFECTIVE HAMILTONIAN

A minimum model of strongly correlated systems with a spin crossover is the two-band Hubbard model. The Hamiltonian of the model can be presented as

$$\hat{H} = \hat{H}_{\Delta} + \hat{H}_t + \hat{H}_{\text{Coulomb}}. \quad (1)$$

Here, the first term

$$\hat{H}_{\Delta} = \varepsilon_1 \sum_{i,\sigma} a_{i,1,\sigma}^{\dagger} a_{i,1,\sigma} + \varepsilon_2 \sum_{i,\sigma} a_{i,2,\sigma}^{\dagger} a_{i,2,\sigma} \quad (2)$$

contains the single-ion energy of electrons in the single-particle states with energy levels ε_1 and $\varepsilon_2 = \varepsilon_1 + \Delta$, where Δ is the energy of electrons in the crystal field (for convenience, we can take $\varepsilon_1 = 0$) and $\sigma = \pm 1/2$ is the electron spin projection. The second term

$$\begin{aligned} \hat{H}_t = & t_{11} \sum_{\langle i,j \rangle, \sigma} a_{i,1,\sigma}^{\dagger} a_{j,1,\sigma} + t_{22} \sum_{\langle i,j \rangle, \sigma} a_{i,2,\sigma}^{\dagger} a_{j,2,\sigma} \\ & + t_{12} \sum_{\langle i,j \rangle, \sigma} (a_{i,2,\sigma}^{\dagger} a_{j,1,\sigma} + a_{i,1,\sigma}^{\dagger} a_{j,2,\sigma}), \end{aligned} \quad (3)$$

where $t_{\lambda\lambda'}$ are the hopping integrals ($\lambda, \lambda' = 1, 2$), describes the electron hopping between nearest-neighbor sites of the crystal lattice with energy levels ε_1 and ε_2 . The third

^{*}jso.krasn@mail.ru

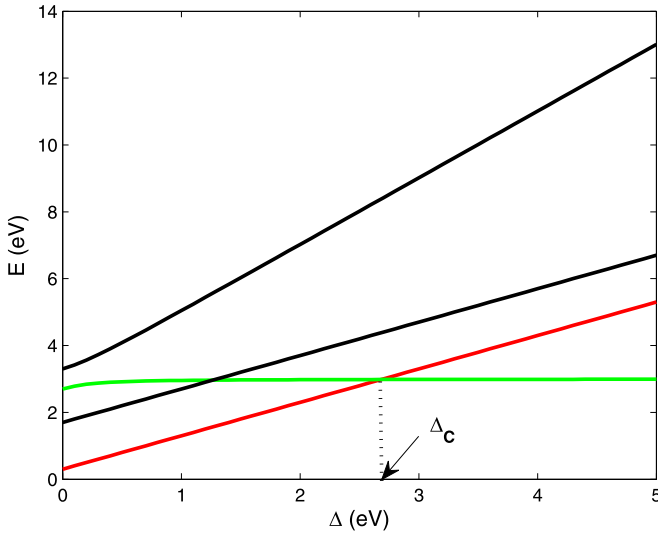


FIG. 1. Dependence of the term energy on crystal field Δ . The red line shows the position of the HS state ($S = 1$) and the green line, the position of the LS state ($S = 0$). The black lines correspond to the excited singlet states. Δ_c is the crossover point. The calculation was made for a set of the Coulomb interaction parameters $U = 3$, $V = 1$, $J_H = 0.7$, and $J'_H = 0.3$ eV.

term

$$\begin{aligned}
 \hat{H}_{\text{Coulomb}} = & U \sum_{i,\lambda} a_{i\lambda\uparrow}^\dagger a_{i\lambda\downarrow}^\dagger a_{i\lambda\uparrow} a_{i\lambda\downarrow} + V \sum_{i,\lambda \neq \lambda'} a_{i\lambda\uparrow}^\dagger a_{i\lambda'\downarrow}^\dagger a_{i\lambda\uparrow} a_{i\lambda'\downarrow} \\
 & + V \sum_{i,\lambda > \lambda', \sigma} a_{i\lambda\sigma}^\dagger a_{i\lambda'\sigma}^\dagger a_{i\lambda\sigma} a_{i\lambda'\sigma} \\
 & + J_H \sum_{i,\lambda > \lambda', \sigma} a_{i\lambda\sigma}^\dagger a_{i\lambda'\sigma}^\dagger a_{i\lambda\sigma} a_{i\lambda'\sigma} \\
 & + J_H \sum_{i,\lambda \neq \lambda'} a_{i\lambda\uparrow}^\dagger a_{i\lambda'\downarrow}^\dagger a_{i\lambda\uparrow} a_{i\lambda'\downarrow} \\
 & + J'_H \sum_{i,\lambda \neq \lambda'} a_{i\lambda\uparrow}^\dagger a_{i\lambda'\downarrow}^\dagger a_{i\lambda\downarrow} a_{i\lambda'\uparrow}
 \end{aligned} \quad (4)$$

contains the one-site energy of the Coulomb interaction of electrons (the electron-electron interaction is considered in the Kanamori approximation [17]).

An important feature of such a two-orbital model is the possibility of forming, at half filling ($N_e = 2$ is the average number of electrons per crystal lattice site) and in the zero approximation over the interstitial hoppings $t_{\lambda\lambda'} = 0$, different localized multielectron (two-particle) states (terms) with the spin $S = 0, 1$ (Fig. 1) and a crossover between them with increasing Δ . In particular, at $N_e = 2$, the Hamiltonian $\hat{H}_\Delta + \hat{H}_{\text{Coulomb}}$ has six eigenstates. In the range of $\Delta < \Delta_c$, the ground state is the triplet ($S = 1$) HS state $|\sigma\rangle$ with the energy $E_{\text{HS}} = 2\varepsilon_1 + \Delta + V - J_H$ (red line in Fig. 1) triply degenerate over the spin projection $\sigma = 0, \pm 1$:

$$|\sigma\rangle = \begin{cases} a_{1\uparrow}^\dagger a_{2\uparrow}^\dagger |0\rangle, & \sigma = +1, \\ \frac{1}{\sqrt{2}}(a_{1\uparrow}^\dagger a_{2\downarrow}^\dagger |0\rangle + a_{1\downarrow}^\dagger a_{2\uparrow}^\dagger |0\rangle), & \sigma = 0, \\ a_{1\downarrow}^\dagger a_{2\downarrow}^\dagger |0\rangle, & \sigma = -1, \end{cases}$$

and, at $\Delta > \Delta_c$, the ground state is the singlet ($S = 0$) LS state $|s\rangle = C_1(\Delta)a_{1\uparrow}^\dagger a_{1\downarrow}^\dagger |0\rangle - C_2(\Delta)a_{2\uparrow}^\dagger a_{2\downarrow}^\dagger |0\rangle$ with the energy $E_{\text{LS}} = 2\varepsilon_1 + (\Delta + U) - \sqrt{\Delta^2 + J_H^2}$ (green line in Fig. 1). At the crossover point $\Delta = \Delta_c = \sqrt{(U - V + J_H)^2 - J_H^2}$, the energy levels of these states cross: $E_{\text{HS}} = E_{\text{LS}}$. The remaining two states are the excited singlet states $|s_1\rangle = \frac{1}{\sqrt{2}}(a_{1\uparrow}^\dagger a_{2\downarrow}^\dagger |0\rangle - a_{1\downarrow}^\dagger a_{2\uparrow}^\dagger |0\rangle)$ and $|s_2\rangle = C_2(\Delta)a_{1\uparrow}^\dagger a_{1\downarrow}^\dagger |0\rangle + C_1(\Delta)a_{2\uparrow}^\dagger a_{2\downarrow}^\dagger |0\rangle$, where $C_1(\Delta) = \sqrt{1 - C_2^2(\Delta)}$, $C_2(\Delta) = x/2(1 + x + \sqrt{1 + x})$ ($x = J_H^2/\Delta^2$) are the normalization coefficients (black lines in Fig. 1).

To derive the effective Hamiltonian, it is convenient to use the Hubbard X operators $X^{p,q} = |p\rangle\langle q|$ [18] constructed on the $\hat{H}_\Delta + \hat{H}_{\text{Coulomb}}$ Hamiltonian eigenstates:

$$(\hat{H}_\Delta + \hat{H}_{\text{Coulomb}})|p\rangle = E_p|p\rangle \quad (5)$$

with different numbers of electrons $N_e = 1, 2, 3$. Since the Hubbard operators form a linearly independent basis, any local operator can be expressed via the linear combination of the X operators, including the single-electron operator of annihilation (creation) on site i with orbital index λ and the spin projection $\sigma = \pm 1/2$:

$$a_{i\lambda\sigma} = \sum_{pq} |p\rangle\langle p| a_{i\lambda\sigma} |q\rangle\langle q| = \sum_{pq} \gamma_{\lambda\sigma}(pq) X_i^{pq}. \quad (6)$$

Since the number of different root vectors (pq) is finite, they can be numbered and put in correspondence with their numbers m [19]; then, we have $a_{i\lambda\sigma} = \sum_m \gamma_{\lambda\sigma}(m) X_i^m$, $a_{i\lambda\sigma}^\dagger = \sum_m \gamma_{\lambda\sigma}^*(m) X_i^{\dagger m}$.

In the representation of the Hubbard X operators, Hamiltonian Eq. (1) has the form

$$\hat{H} = \sum_{i,p} E_p X_i^{pp} + \sum_{(i,j)} \sum_{mn} t^{mn} X_i^{\dagger m} X_j^n. \quad (7)$$

Here, E_p is the energy of many-electron terms and $t_{mn} = \sum_{\sigma,\lambda,\lambda'} t_{\lambda\lambda'} \gamma_{\lambda\sigma}^*(m) \gamma_{\lambda'\sigma}(n)$ is the renormalized hopping integral.

Using Hamiltonian Eq. (7) as the initial one, we can obtain the effective Hamiltonian by excluding the interband hoppings from it. To do that, we use the projection operator method developed in [20] for the Hubbard model and in [21] for the p - d model (see also [5,8]). The effective Hamiltonian has the form

$$\hat{H}_{\text{eff}} = \hat{H}_S + \hat{H}_{\text{nn}} + \hat{H}_{\text{ex}}. \quad (8)$$

Here, the first term contains the exchange contribution to the Heisenberg Hamiltonian with allowance for the energy of the electronic configurations of the LS and HS states

$$\begin{aligned}
 \hat{H}_S = & \frac{1}{2} J \sum_{(i,j)} \left(\hat{S}_i \cdot \hat{S}_j - \frac{1}{4} \hat{n}_i \hat{n}_j \right) + E_{\text{LS}} \sum_i X_i^{s,s} \\
 & + E_{\text{HS}} \sum_{i,\sigma} X_i^{\sigma,\sigma},
 \end{aligned} \quad (9)$$

where \hat{S}_i is the spin operator for $S = 1$: $\hat{S}_i^+ = \sqrt{2}(X_i^{+1,0} + X_i^{0,-1})$, $\hat{S}_i^- = \sqrt{2}(X_i^{0,+1} + X_i^{-1,0})$, $\hat{S}_i^z = X_i^{+1,+1} - X_i^{-1,-1}$

[22]; $J = (t_{11}^2 + 2t_{12}^2 + t_{22}^2)/\Omega_g$ is the exchange integral; Ω_g is the energy gap between the centers of the upper and lower Hubbard subbands [20,21]; and $\hat{n}_i = 2(X_i^{s,s} + \sum_{\sigma} X_i^{\sigma,\sigma}) = 2(\hat{n}_i^{LS} + \hat{n}_i^{HS})$ is the particle number operator at site i [$\hat{n}_i^{LS(HS)}$ is the particle number operator in the LS(HS) state]. Here, $\sigma = 0, \pm 1$. Using the completeness condition $X^{s,s} + \sum_{\sigma} X^{\sigma,\sigma} = 1$, we can show $\langle \hat{n}_i \rangle = 2(\langle \hat{n}_i^{LS} \rangle + \langle \hat{n}_i^{HS} \rangle) = 2(n_{LS} + n_{HS}) = 2$; hereinafter, angular brackets $\langle \dots \rangle$ mark the thermodynamic average and $n_{LS(HS)}$ is the occupation number of the LS (HS) state ($n_{LS} + n_{HS} = 1$). If we introduce spin gap ε_S that is the difference $E_{HS} - E_{LS}$, then Eq. (9) can be presented in the form

$$\hat{H}_S = \frac{1}{2}J \sum_{(i,j)} \left(\hat{S}_i \cdot \hat{S}_j - \frac{1}{4} \hat{n}_i \hat{n}_j \right) - \varepsilon_S \sum_i X_i^{s,s} + NE_{HS}, \quad (10)$$

where N is the number of crystal lattice sites; $\varepsilon_S = 0$ corresponds to the spin crossover. The spin gap depends on pressure; it is negative in the HS state and positive in the LS state, and at the critical pressure P_{C0} the spin gap is zero in the simplest single-site picture. Below we will show that the effects of cooperativity given by the other terms in Eq. (8) will shift the crossover point and pressure to the value $P_C > P_{C0}$.

The second term in Eq. (8) describes the density-density interaction of the LS states

$$\hat{H}_{nm} = \frac{1}{2} \tilde{J} \sum_{(i,j)} X_i^{s,s} \cdot X_j^{s,s}, \quad (11)$$

where $\tilde{J} = [1 - (2C_1C_2)^2](t_{11}^2 - 2t_{12}^2 + t_{22}^2)/\Omega_g$.

The third term in Eq. (8) contains the interatomic exciton hopping with an amplitude J'_{ex} and biexciton creation/annihilation with an amplitude J''_{ex} ,

$$\hat{H}_{ex} = \sum_{(i,j)} \sum_{\sigma} \left[\frac{1}{2} J'_{ex} (X_i^{\sigma,s} X_j^{s,\sigma} + X_i^{s,\sigma} X_j^{\sigma,s}) - \frac{1}{2} J''_{ex} (-1)^{|\sigma|} (X_i^{\sigma,s} X_j^{\bar{\sigma},s} + X_i^{s,\sigma} X_j^{s,\bar{\sigma}}) \right], \quad (12)$$

where $J'_{ex} = 2C_1C_2(t_{11}t_{22} - t_{12}^2)/\Omega_g$, $J''_{ex} = (t_{11}t_{22} - t_{12}^2)/\Omega_g$, and $\bar{\sigma} = -\sigma$. In Eq. (12), the Hubbard operators $X_i^{\sigma,s}$ and $X_i^{s,\sigma}$ on site i describe the spin excitons, the Bose excitations from the LS singlet state $|s\rangle$ to the HS triplet state $|\sigma\rangle$ with a spin projection of $\sigma = 0, \pm 1$, and vice versa.

It can be seen from Fig. 1 that the energy of the LS term is practically independent of the crystal field. The dependence on Δ and deviation from the linear dependence takes place at small Δ ($\Delta \leq J'_H$). Therefore, in a fairly wide region near the spin crossover (at $\Delta > J'_H$), we have $C_1 \approx 1$, but $C_2 \approx 0$; therefore, $J'_{ex} \approx 0$. Hereinafter we use hopping parameters of $t_{11} = t_{22} = 1$ eV and $t_{12} = 0.5$ eV, for which the relations $\tilde{J}/J = 0.6$ and $J''_{ex}/J = 0.3$ are valid.

Introducing the designations $d_x = \frac{1}{\sqrt{2}}(-d_+ + d_-)$, $d_y = \frac{1}{\sqrt{2}}(d_+ + d_-)$, and $d_z = d_0$, where $d_+ = X^{s,+}$, $d_- = X^{s,-}$,

and $d_0 = X^{s,0}$, we can rewrite Eq. (12) in the form

$$\hat{H}_{ex} = \frac{1}{2} J'_{ex} \sum_{(i,j)} (\mathbf{d}_i^\dagger \cdot \mathbf{d}_j + \text{H.c.}) - \frac{1}{2} J''_{ex} \sum_{(i,j)} (\mathbf{d}_i^\dagger \cdot \mathbf{d}_j^\dagger + \text{H.c.}) \quad (13)$$

In the mean-field (MF) approximation, for two sublattices A and B we have

$$\hat{H}_{\text{eff}}^{\text{MF}} = \hat{H}_S^{\text{MF}} + \hat{H}_{ex}^{\text{MF}} + \hat{H}_{nm}^{\text{MF}}, \quad (14)$$

where

$$\begin{aligned} \hat{H}_S^{\text{MF}} &= Jz m_B \sum_{i_A} \hat{S}_{i_A}^z + Jz m_A \sum_{i_B} \hat{S}_{i_B}^z \\ &- Jz \sum_{i_A} \hat{n}_{i_A} - Jz \sum_{i_B} \hat{n}_{i_B} - \varepsilon_S \sum_{i_A} X_{i_A}^{s,s} - \varepsilon_S \sum_{i_B} X_{i_B}^{s,s} \\ &- \frac{1}{2} Jz N m_A m_B + \frac{1}{2} Jz N + NE_{HS}, \quad (15) \\ \hat{H}_{nm}^{\text{MF}} &= \tilde{J} z n_B^{LS} \sum_{i_A} \hat{n}_{i_A}^{LS} + \tilde{J} z n_A^{LS} \sum_{i_B} \hat{n}_{i_B}^{LS} \\ &- \tilde{J} z \frac{N}{2} n_A^{LS} n_B^{LS}, \quad (16) \end{aligned}$$

and

$$\begin{aligned} \hat{H}_{ex}^{\text{MF}} &= \sum_F \sum_{\sigma=\pm 1,0} \left\{ J'_{ex} z \Delta_F^\sigma \sum_{i_F} (X_{i_F}^{s,\sigma} + X_{i_F}^{\sigma,s}) \right. \\ &- (-1)^{|\sigma|} J''_{ex} z \Delta_F^\sigma \sum_{i_F} (X_{i_F}^{s,\bar{\sigma}} + X_{i_F}^{\bar{\sigma},s}) \\ &\left. - \frac{1}{2} z N (J'_{ex} \Delta_F^\sigma \Delta_F^\sigma - (-1)^{|\sigma|} J''_{ex} \Delta_F^\sigma \Delta_F^{\bar{\sigma}}) \right\}. \quad (17) \end{aligned}$$

Here, z is the number of nearest neighbors; $F = A, B$ ($\bar{F} = A$, if $F = B$ and vice versa); $m_{A(B)} = \langle \hat{S}_{i_{A(B)}}^z \rangle$ is the magnetization of sublattice A (B); $\Delta_{A(B)}^+ = \langle X_{i_{A(B)}}^{s,+} \rangle$, $\Delta_{A(B)}^- = \langle X_{i_{A(B)}}^{s,-} \rangle$, and $\Delta_{A(B)}^0 = \langle X_{i_{A(B)}}^{s,0} \rangle$ are the components of the exciton order parameters, for which the equalities $(\Delta^+)^{\dagger} = \langle X^{+,s} \rangle = \Delta^+$, $(\Delta^-)^{\dagger} = \langle X^{-,s} \rangle = \Delta^-$, and $(\Delta^0)^{\dagger} = \langle X^{0,s} \rangle = \Delta^0$ are valid under the thermodynamic equilibrium. It should be noted that the nonzero average $\Delta^{+/-} \neq 0$ indicates the quantum-mechanical mixing of the LS and HS states, but in the absence of the spin-orbit coupling.

III. PHASE DIAGRAMS IN THE PLANE (SPIN GAP, TEMPERATURE)

Solving the problem on the eigenvalues

$$\hat{H}_{\text{eff}}^{\text{MF}} |\psi\rangle_k = E_k |\psi\rangle_k, \quad (18)$$

where $|\psi\rangle_k = C_{LS,k}|s\rangle + \sum_{\sigma} C_{HS,k}|\sigma\rangle$ are the eigenstates of Hamiltonian Eq. (14), and using the solutions corresponding to the minimum free energy $F = -k_B T \ln Z$, where $Z = \sum_k e^{-E_k/k_B T}$ is the system partition function, we can calculate different thermodynamic averages.

Figure 2 shows the calculated phase diagrams of the magnetization and population of the HS state for the two

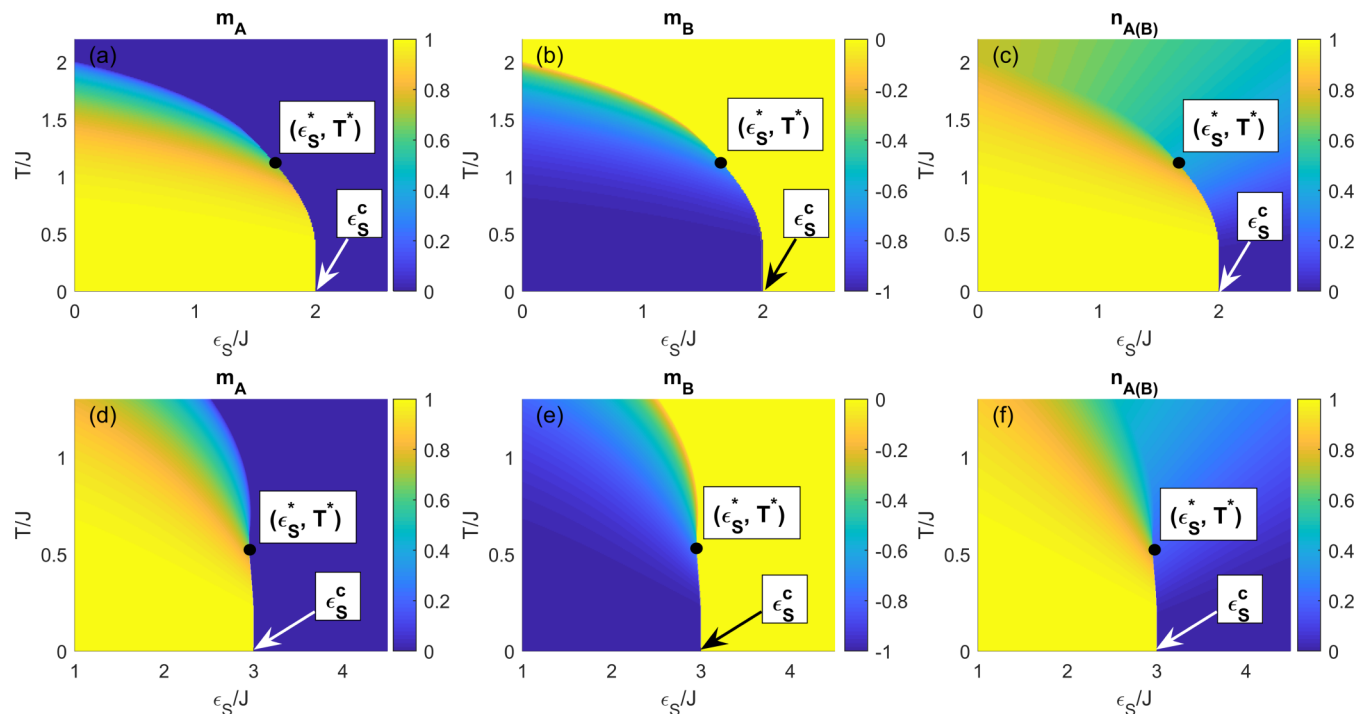


FIG. 2. Phase diagrams of (a), (b), (d), (e) the magnetization and (c), (f) populations of the HS state for two sublattices at $J''_{ex} = 0$ and $\tilde{J} = 0$ (the upper row) and $\tilde{J} = 0.6J$ (the lower row).

sublattices at $J''_{ex} = 0$ and $\tilde{J} = 0$ (the upper row) and $\tilde{J} = 0.6J$ (the lower row) in the coordinates temperature T –spin gap ε_S . The calculation was made at $J = 28$ K [23]. Hereinafter, the temperature and spin gap are given in terms of exchange parameter J . First, we consider the case $\tilde{J} = 0$ illustrated in Fig. 2 (the upper row). It can be seen that, due to the presence of the cooperative exchange coupling J , the ground magnetically ordered HS-AFM state is preserved in a system up to $\varepsilon_S = \varepsilon_S^c \approx 2J$ [Figs. 2(a)–2(c)], although in the single-ion picture at $\varepsilon_S > 0$, the LS state is ground. The growth of the critical ε_S^c value by the expense of the cooperative effects is quite clear, since the exchange coupling stabilizes the HS state via lowering its energy. At $\varepsilon_S > \varepsilon_S^c$, the ground HS-AFM state changes for the nonmagnetic LS state [Figs. 2(a) and 2(b)].

In the range of $\varepsilon < \varepsilon_S^c$ [Figs. 2(a) and 2(b)], with increasing temperature, the system undergoes a second-order phase transition from the HS-AFM state to the paramagnetic state at $\varepsilon_S < \varepsilon_S^*$ and a first-order transition at $\varepsilon_S^* < \varepsilon_S < \varepsilon_S^c$. In the diagram, one can clearly see the existence of a tricritical point [T^* and ε_S^* in Figs. 2(a)–2(c)], at which the line of the second-order phase transitions continuously passes to the line of the first-order ones.

At $\tilde{J} = 0.6J$ (the lower row in Fig. 2), the phase diagram is qualitatively similar to the case illustrated in Figs. 2(a)–2(c), but the region of existence of the long-range antiferromagnetic order ($\varepsilon_S^c \approx 3J$) increases. This is due to the fact that the LS density-density interatomic interaction Eq. (11) stabilizes the HS state.

At $J''_{ex} = 0.3J$, the phase diagram becomes richer (Figs. 3 and 4). Figure 3 shows the calculated phase diagrams of population n_{HS} of the HS state (the upper row), magnetization m

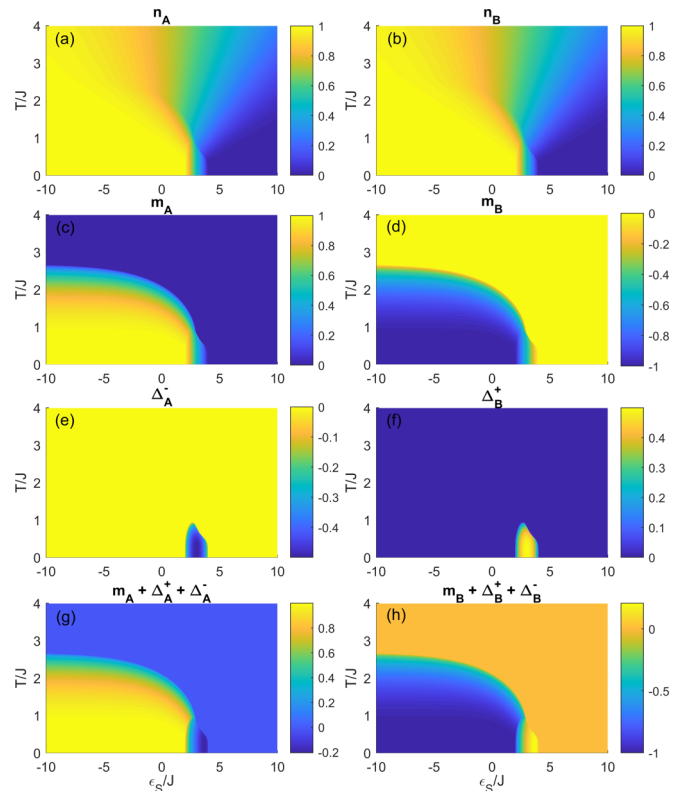


FIG. 3. Calculated phase diagrams of (a), (b) population n of the HS state, (c), (d) magnetization m , (e), (f) exciton order parameter components Δ , and (g), (h) sum $m + \Delta$ for sublattices A (on the left) and B (on the right).

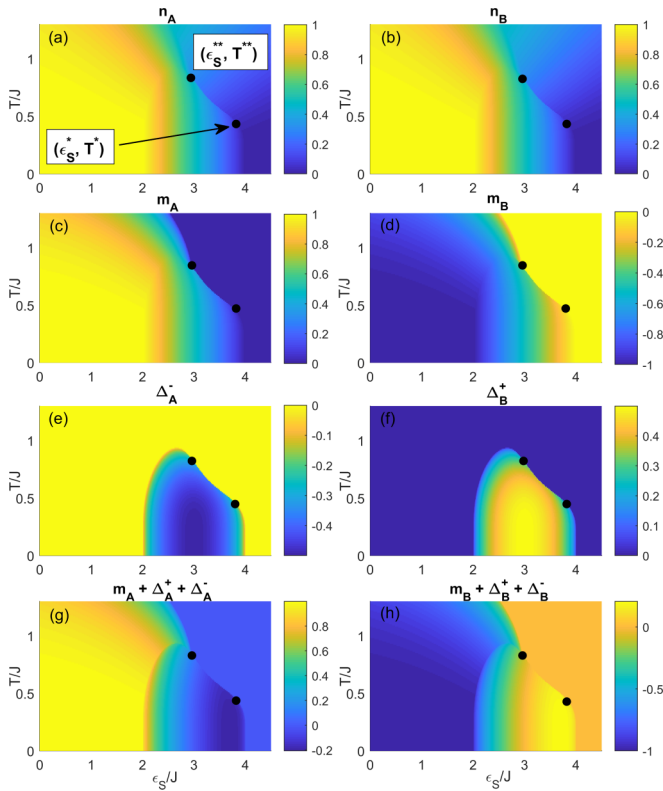


FIG. 4. Figure 3 on an enlarged scale.

(the second row), exciton order parameter components $\Delta^{+/-}$ (the third row), and the sum $m + \Delta^{+/-}$ (the lower row) for two sublattices A (on the left) and B (on the right) in the coordinates temperature T –spin gap ε_S . It can be seen that $n_{HS,A} = n_{HS,B}$ [Figs. 3(a) and 3(b)]; $m_A = -m_B$, the long-range antiferromagnetic order is implemented in a system [Figs. 3(c) and 3(d)]; $\Delta_A^- = -\Delta_B^+$ [Figs. 3(e) and 3(f)], in this case, we have $\Delta_A^+ = \Delta_B^- = 0$. Figure 4 contains Fig. 3 on an enlarged scale.

Near ε_S^c , the exciton condensate region arises, which coexists with the long-range antiferromagnetic order. Moreover, the comparison of Fig. 4 and Fig. 2 (the lower row) shows that the formation of the exciton condensate facilitates the antiferromagnetic ordering and the occurrence of the magnetization in the range of parameters T and ε_S where there was no magnetic order at $J''_{ex} = 0$ [Figs. 2(d) and 2(e)]. This can be clearly seen in Fig. 5, which shows the temperature dependence of population n of the HS state [Fig. 5(a)], magnetization m [Fig. 5(b)], and the exciton order parameter components $\Delta^{+/-}$ [Fig. 5(c)] for the two sublattices and the derivative of minimum free energy F [Fig. 5(d)] at $\varepsilon_S/J = 3.5 > \varepsilon_S^c/J \approx 3$ (see above). For comparison, Fig. 5 (the right column) presents temperature dependencies of the same quantities, but at $J''_{ex} = 0$. Due to the formation of an exciton condensate at low temperatures [Fig. 5(c)], a nonzero HS state population appears [Fig. 5(a)] and the magnetization [Fig. 5(b)], which abruptly vanishes with increasing temperature (the first derivative of the free energy [Fig. 5(d)] reveals a jump, which corresponds to a first-order phase transition). Physically, this is quite clear from the structure of the exciton order parameter.

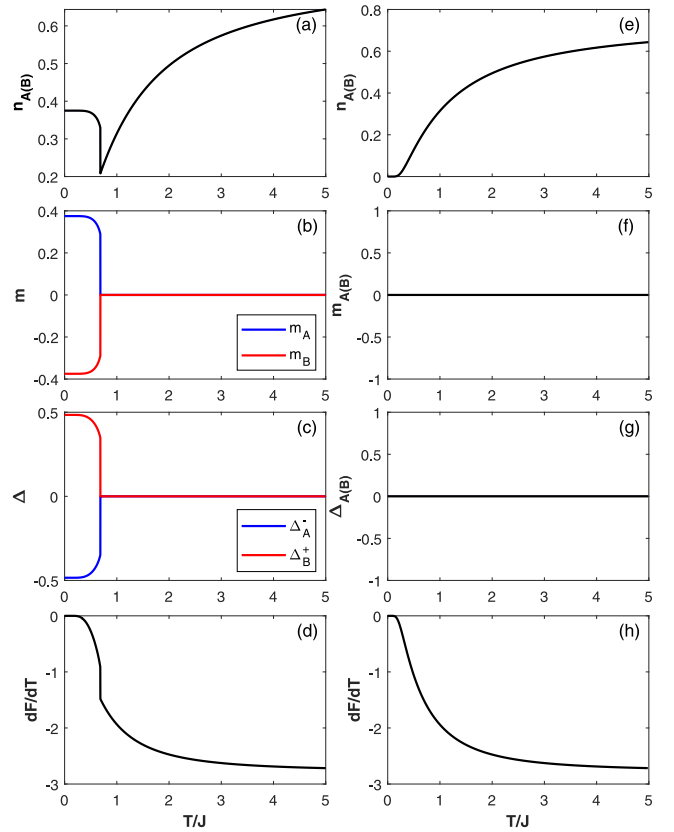


FIG. 5. Temperature dependencies of (a) population n of the HS state, (b) magnetization m and (c) exciton order parameter components $\Delta^{+/-}$ for two sublattices, and temperature derivative of minimum free energy F (d) at $\varepsilon_S/J = 3.5 > \varepsilon_S^c/J \approx 3$, $J''_{ex} = 0.3J$ (the left column), and $J''_{ex} = 0$ (the right column).

In particular, at $\Delta_A^- \neq 0$, we have $\Delta_A^+ = 0$; then, $\Delta_B^+ = -\Delta_A^-$ and $\Delta_B^- = 0$. On the contrary, at $\Delta_A^+ \neq 0$, we have $\Delta_A^- = 0$; then, $\Delta_B^- = -\Delta_A^+$ and $\Delta_B^+ = 0$. The nonzero corresponding values $\Delta^{+/-}$ on different sublattices allow the coexistence of an exciton condensate with antiferromagnetism and facilitates its formation.

Interaction parameters J , \tilde{J} , and J_{ex} are determined by the hopping parameters (see above). In this problem, all three parameters are positive; however, it is technically interesting to study the structure of the exciton order parameter at different signs of parameters J and J_{ex} (near the crossover J''_{ex}), including the case of $J = 0$. The parameter \tilde{J} determines the range of stability of the HS (LS) state and does not effect the exciton order parameter. Table I gives the values and signs of the components of the pseudovector $\langle \mathbf{d} \rangle = \{\Delta^+, \Delta^-, \Delta^0\}$ in the minimum of thermodynamic potential F . The case $J > 0$ corresponds to the antiferromagnetic ordering; in this case, in the crossover region the exciton condensate phase coexists with the antiferromagnetism and facilitates it. At $J < 0$, the ferromagnetic ordering is implemented in the system, but the ferromagnetism and the exciton condensate phase are separated and cannot coexist. Finally, at $J = 0$, vector $\langle \mathbf{d} \rangle$ has the same structure as at $J < 0$ and does not facilitate the occurrence of magnetism; the presence of component Δ^+ is compensated by the action of Δ^- and vice versa on each

TABLE I. Structure of the exciton order parameter at the minimum of free energy for different signs of the exchange J and exciton J''_{ex} interaction parameters. Here, we used the following designations: signs + (−) and 0 mean that the component is positive (negative) or zero, respectively; the sign / means “or”, and A and B are two sublattices. At any combination of J and J''_{ex} , if the components are nonzero, they have the same absolute value.

	$J > 0$				$J \leq 0$			
	$J''_{ex} > 0$		$J''_{ex} < 0$		$J''_{ex} > 0$		$J''_{ex} < 0$	
	A	B	A	B	A	B	A	B
Δ^+	0	+/-	0	+	-	+	+	+
Δ^-	-/+	0	+	0	-	+	+	+
Δ^0	0	0	0	0	+	+	-	+

lattice site. It should be noted that at $J < 0$ and $J = 0$, there is no partitioning into magnetic sublattices, but there is the partitioning caused by the structure (“direction”) of the order parameter $\langle \mathbf{d} \rangle$.

Along with the tricritical point (T^* and ε_S^* in Fig. 4 and Fig. 2), the phase diagram contains a bicritical point in (T^{**} and ε_S^{**} in Fig. 4), at which the second-order phase transition line splits into two second- and first-order phase transition lines (Fig. 4), according to the Gibbs phase rule.

In closing this section, we would like to compare our results with the data on the exciton ferromagnetism reported in [24], where the authors discussed the electron-phonon interaction, along with the electron-electron one. The situation can be briefly described as follows. As is known, the spin density wave (SDW) magnetic structure is implemented in the metals in which the topology of the multiply connected Fermi surface contains electron and hole regions, which coincide upon parallel transfer to certain vector \mathbf{q} . The SDW arises due to triplet pairing of single-particle excitations of the coinciding electron and hole regions of the Fermi surface. If the SDW is superimposed onto the charge density wave (CDW) already present in the system and induced by singlet pairing of the electron and hole states, the picture becomes more complex. The coexisting single-phase commensurate SDW and CDW induce additional magnetic splitting of the single-particle excitation spectrum, which results in the occurrence of a magnetic moment per unit crystal volume upon doping (the so-called excitonic ferromagnetism). In this work, by analogy with [24], we can speak about the exciton antiferromagnetism, at which the formation of an exciton phase facilitates the occurrence of a long-range antiferromagnetic order in the region of phase diagram where the AFM phase would be absent above critical value of the spin gap (pressure) without the excitonic condensate.

IV. ELECTRON BAND STRUCTURE IN DIFFERENT PHASES

To obtain the dispersion relations for the quasiparticle excitations, we use the method of equations of motion for the matrix Green’s function $D_{mn}(\mathbf{k}, \omega) = \langle \langle X_{\mathbf{k}}^m | X_{\mathbf{k}}^{\dagger n} \rangle \rangle_{\omega}$ related to the single-electron Green’s function $G_{\lambda\sigma}(\mathbf{k}, \omega) = \langle \langle a_{\mathbf{k}\lambda\sigma} | a_{\mathbf{k}\lambda\sigma}^{\dagger} \rangle \rangle_{\omega}$, where $\sigma = \pm 1/2$ is the electron spin projec-

tion, as

$$G_{\lambda\sigma}(\mathbf{k}, \omega) = \sum_{m,n} \gamma_{\lambda\sigma}(m) \gamma_{\lambda\sigma}^*(n) D_{mn}(\mathbf{k}, \omega). \quad (19)$$

Here, as in Eq. (6), X are the Hubbard operators constructed using the eigenstates Eq. (5) for $N_e = 1, 3$, while at $N_e = 2$ eigenstates Eq. (18) are used.

The spectral density of the single-particle excitations is expressed through the Fermi single-particle Green’s function

$$\begin{aligned} A_{\lambda\sigma}(\mathbf{k}, \omega) &= -\frac{1}{\pi} \text{Im} G_{\lambda\sigma}(\mathbf{k}, \omega + i\delta) \\ &= -\frac{1}{\pi} \text{Im} \sum_{mn} \gamma_{\lambda\sigma}(m) \gamma_{\lambda\sigma}^*(n) D_{mn}(\mathbf{k}, \omega + i\delta), \\ \delta &\rightarrow +0, \end{aligned} \quad (20)$$

and the density of the single-particle states for a specified spin projection (N_k is the normalization factor, the number of points in the Brillouin zone) is $N_{\lambda\sigma}(\omega) = \frac{1}{N_k} \sum_{\mathbf{k}} A_{\lambda\sigma}(\mathbf{k}, \omega)$.

In the diagram technique for X operators, we can write the Dyson equation for the Green’s function $\hat{D}(\mathbf{k}, \omega)$ [25]

$$\hat{D}(\mathbf{k}, \omega) = [\hat{G}_0^{-1}(\omega) - \hat{P}(\mathbf{k}, \omega) \hat{t}(\mathbf{k}) + \hat{\Sigma}(\mathbf{k}, \omega)]^{-1} \hat{P}(\mathbf{k}, \omega). \quad (21)$$

Here, $\hat{\Sigma}(\mathbf{k}, \omega)$ and $\hat{P}(\mathbf{k}, \omega)$ are the self-energy and force operators, respectively, and $G_{0mn}(\omega) = \delta_{mn}(\omega - \Omega_m)^{-1}$. In the Hubbard-I approximation, the structure of the exact Green’s function Eq. (21) is preserved, but the self-energy operator is set to be zero and the force operator, to be $P_{mn}(\mathbf{k}, \omega) \rightarrow \delta_{mn} F_m$.

In the Hubbard-I approximation for the Green’s function $\hat{D}(\mathbf{k}, \omega)$, we can write the equation

$$\hat{D}(\mathbf{k}, \omega) = \hat{D}_0(\omega) + \hat{D}_0(\omega) \hat{t}(\mathbf{k}) \hat{D}(\mathbf{k}, \omega). \quad (22)$$

Here, $D_0^{mn}(\omega) = \delta_{mn} F_m / (\omega - \Omega_m)$, where $\Omega_m \equiv \Omega(pq) = E_p - E_q$; $F_m \equiv F(pq) = \langle X^{pp} \rangle + \langle X^{qq} \rangle$ is the filling factor called the end factor in the diagram technique for X operators [19]; $t_{mn}(\mathbf{k}) = \sum_{\sigma, \lambda, \lambda'} \gamma_{\lambda\sigma}(m) \gamma_{\lambda\sigma}^*(n) t_{\lambda\lambda'}(\mathbf{k})$, where $t_{\lambda\lambda'}(\mathbf{k})$ is the Fourier transform of the hopping integrals. The solution of Eq. (22) has the form $\hat{D}^{-1}(\mathbf{k}, \omega) = \hat{D}_0^{-1}(\omega) - \hat{t}(\mathbf{k})$, which is typical for the MF theory.

The dispersion dependence of the Fermi quasiparticles is determined by the equation for a pole of the matrix Green’s function $D_{mn}(\mathbf{k}, \omega) = \{[\hat{D}_0^{-1}(\omega) - \hat{t}(\mathbf{k})]^{-1}\}_{mn}$:

$$\det \|\delta_{mn}(\omega - \Omega_m) / F_m - t_{mn}(\mathbf{k})\| = 0. \quad (23)$$

The form of this equation is similar to the dispersion equation of the tight-binding method in the one-electron band theory, but differs from it by the two circumstances: first, indices m and n number the single-particle excitations in a many-electron system rather than one-electron orbitals, and second, the effective hopping parameter is determined by the product $t_{mn}(\mathbf{k})$ and filling factor F_m , which depends on the occupation numbers of the initial and final states (for more details, see [26]).

It is noteworthy that a consequence of exact representation Eq. (6) and commutation relations for the Fermi operators is the sum rule $\langle [a_{i,\lambda,\sigma}, a_{i,\lambda,\sigma}^{\dagger}]_+ \rangle = 1 = \sum_m |\gamma_{\lambda\sigma}(m)|^2 F(m)$.

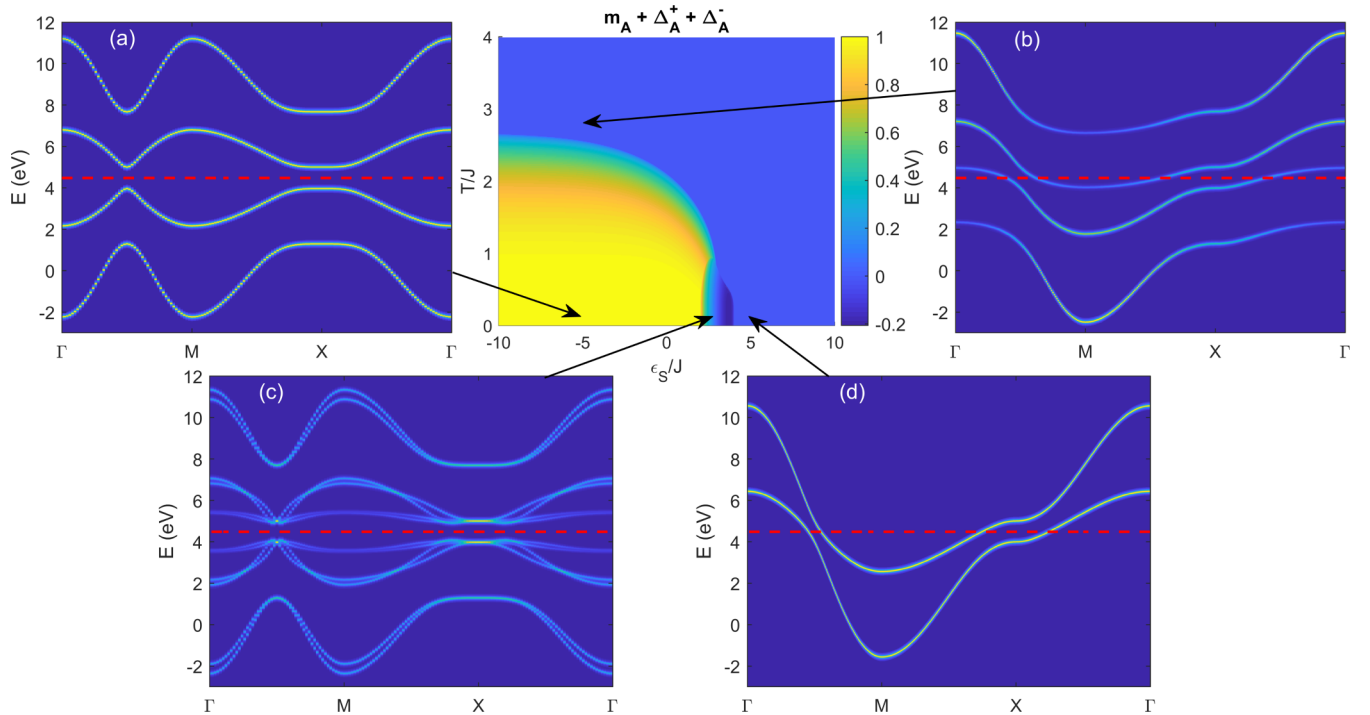


FIG. 6. Electron band structure at half filling ($N_e = 2$ is the average number of electrons per crystal lattice site) along the symmetric directions of the paramagnetic Brillouin zone in different phases (at the center): (a) HS-AFM ($T/J = 0.1$, $\varepsilon_S/J = -5.0$) is an antiferromagnetic insulator, (b) HS-PM ($T/J = 2.8$ and $\varepsilon_S/J = -5.0$) is a paramagnetic semimetal, (c) HS-AFM-Ex ($T/J = 0.1$, $\varepsilon_S/J = 2.5$) is an antiferromagnetic excitonic insulator, and (d) LS ($T/J = 0.1$, $\varepsilon_S/J = 5.0$) is a nonmagnetic semimetal. The red dashed horizontal line shows the position of the chemical potential. Colors show the distribution of the total spectral weight of quasiparticle excitations inside the first Brillouin zone. The central figure shows the phase diagram in Fig. 3(g). $\Gamma(0, 0)$, $M(1, 1)$, and $X(1, 0)$ are the high-symmetry points of the paramagnetic Brillouin zone.

This sum rule results in the conservation of the total spectral weight in each zone λ for any wave vector \mathbf{k} : $\sum_{\sigma} \int A_{\lambda\sigma}(\mathbf{k}, \omega) d\omega = 2$.

Figure 6 shows the modification of the electronic spectrum at half filling ($N_e = 2$ is the average number of electrons per crystal lattice site) in different phases depending on T and ε_S . For example, in the HS-AFM and HS-AFM-Ex phases, the calculated band structure has direct dielectric gap E_g and the Fermi energy lies inside the forbidden band [Figs. 6(a) and 6(c)]. Hereinafter, the distributions of the total spectral weight $A(\mathbf{k}, \omega) = \sum_{\lambda,\sigma} A_{\lambda\sigma}(\mathbf{k}, \omega)$ of the Fermi quasiparticle excitations inside the first Brillouin zone are shown by different colors. Since, in the HS phase, the system is considered in the antiferromagnetic or paramagnetic state and, in the LS phase, in the nonmagnetic state, we everywhere have $A_{\lambda\uparrow}(\mathbf{k}, \omega) = A_{\lambda\downarrow}(\mathbf{k}, \omega)$. The red dashed horizontal line shows the Fermi level position. The occurrence of the spontaneous antiferromagnetic ordering and condensation of magnetic excitons doubles the crystal lattice period, but for convenience of comparing different cases (with and without order), we build the electronic spectrum using the unreduced Brillouin zone. With increasing temperature or spin gap (crystal field), dielectric gap E_g vanishes from the spectrum continuously or stepwise, depending on the order of the phase transition (Fig. 4), and a system passes to the semimetal state [Figs. 6(b) and 6(d)]. In [27], we discussed the topological features of the transition HS semimetal–LS semimetal in the absence of any thermodynamic order parameters.

The number of different quasiparticle bands in Fig. 6 is determined by the number of possible single-electron excitations between multielectron terms. In our two-band model with $N_e = 2$ the relevant configurations are d^2 with $S = 1$ and $S = 0$, d^1 with two orbitals and $S = 1/2$, and d^3 with two orbitals and $S = 1/2$ (Fig. 7). In the excitonic phase the

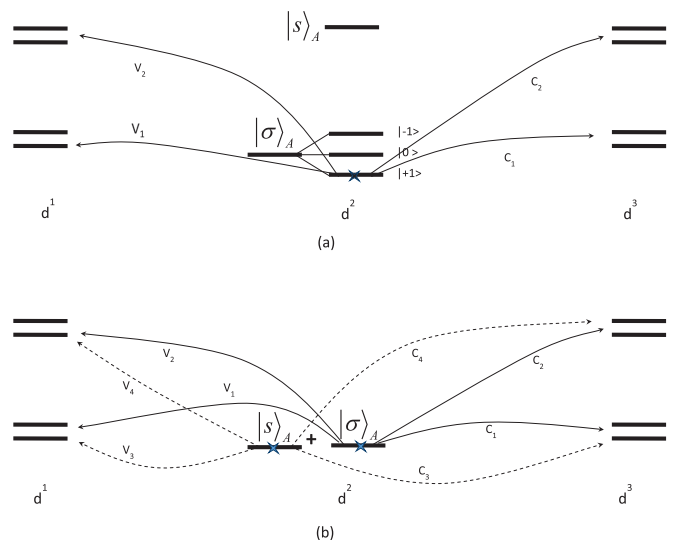


FIG. 7. A scheme of the relevant eigenstates in the HS-AFM phase (a) and in the Ex phase (b).

ground state is given by

$$|0\rangle_A = u|s\rangle_A + v|-1\rangle_A. \quad (24)$$

From Fig. 7 it is clear that in the HS state there are 4 Fermi-type single-electron quasiparticles (excitations from d^2 to d^3 configurations which correspond to the electron creation, and from d^2 to d^1 excitations corresponding hole creation). It is valid both for the paramagnetic HS metal and antiferromagnetic insulator. We want to stress that metallicity of the paramagnetic HS phase is related with its two-band character. Due to strong correlations each single-particle band is split on the upper and low Hubbard subbands, which may cross the Fermi level as in Fig. 6(b) or may form an insulator for smaller hopping parameters. In the excitonic phase the number of possible single-electron excitations is doubled due to its degeneracy; the matrix elements of the electron creation/annihilation in Eq. (6) are nonzero for both singlet and triplet two-electron terms. Nevertheless for $\varepsilon_S \gg \varepsilon_S^C$ the parameter $C_2 = 0$ and the ground singlet is formed by only one orbital, $|s\rangle = a_{1\uparrow}^\dagger a_{1\downarrow}^\dagger |0\rangle$, so the electron addition is possible only for orbital 2, and the electron removal involves only orbital 1. That is why the number of the quasiparticle bands in the LS case [Fig. 6(d)] is only 2. This nonmagnetic phase indeed has paramagnetic properties due to the Pauli susceptibility in the metallic state.

To conclude this section, we would like to discuss the relation between the spin crossover and the effective electron correlation parameter. It is well known that in multiorbital systems (for example, oxides of $3d$ metals), a measure of the electron interaction energy and electron correlations is the effective Hubbard parameter $U_{\text{eff}}(d^n) = E_0(d^{n+1}) + E_0(d^{n-1}) - 2E_0(d^n)$ [28], where $E_0(d^n)$ is the energy of the main term of the d^n configuration. The average number of electrons is assumed to be $\langle n_d \rangle = n$. The competition of the intra-atomic Hund's exchange coupling J_H and the cubic component of the crystal field $10Dq$ for the d^n electron configuration ($n = 4-7$) results in the change in the ground HS/LS state [29]. The HS-LS spin crossover can occur due to the growth of the crystal field, for example, with pressure. As a result, the spin crossover changes $U_{\text{eff}}(d^n)$ and causes the relation to the Mott-Hubbard transition. The effect of the spin crossover on the electron correlation parameter turned out to be nonuniversal: for d^5 ions, U_{eff} is suppressed, while for d^6 it, on the contrary, increases due to the spin crossover and, in the case of d^7 , does not change [30–34]. For the two-band Hubbard model investigated in this work, we neglect the intra-atomic exchange coupling component J'_H [this approximation is justified within a fairly wide crystal field range, for which E_{LS} can be considered independent of Δ (Fig. 1)] and, at half filling, $U_{\text{eff}} = V + |\varepsilon_S|$. It can be clearly seen that, in the HS state ($\Delta < \Delta_c$ in Fig. 1), U_{eff} decreases with increasing crystal field Δ ($|\varepsilon_S|$ decreases), while at $\Delta > \Delta_c$ (the ground LS state) U_{eff} , on the contrary, increases with the crystal field Δ ($|\varepsilon_S|$ increases). Thus, at the spin crossover, the kink of the parameter U_{eff} is observed.

V. DISCUSSION AND CONCLUSIONS

Based on Eq. (1), we can distinguish two cases. In the first (weakly correlated) case, at $\hat{H}_{\text{Coulomb}} \ll \hat{H}_\Delta + \hat{H}_t$, we

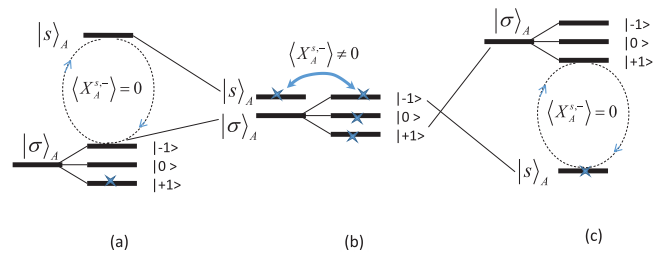


FIG. 8. The energy level scheme for the antiferromagnetic A sublattice for three areas of the spin gap parameter: (a) in the HS state when $\varepsilon_S \ll \varepsilon_S^C$, (b) in the spin crossover region $\varepsilon_S \sim \varepsilon_S^C$, (c) in the LS state $\varepsilon_S \gg \varepsilon_S^C$. The HS triplet level is split in the antiferromagnetic phase, and a cross denotes occupied at zero-temperature level. In both (a) and (c) a spin excitation requires some finite energy and the static excitonic order parameter is zero. Close to spin crossover in (b) triplet level magnetic splitting tends to zero. Two terms, the LS and the HS with projection -1 in the A sublattice, become degenerate and spin excitation energy tends to zero.

have a two-band semiconductor or a semimetal (depending on the ratio between Δ and t), in which an exciton condensate can form according to the Bose-Einstein condensation (BEC) or Bardeen-Cooper-Schrieffer (BCS) scenario. In the second case (strongly correlated), when the energy of the Coulomb interaction of electrons is larger than their kinetic energy and becomes comparable with the energy of the crystal field $\hat{H}_{\text{Coulomb}} \sim \hat{H}_\Delta$, the spin crossover and the formation of localized magnetic excitons become possible. In this study, we showed using the two-band Hubbard-Kanamori model that there is a condensation of such excitons near the spin crossover, which, in turn, leads to the opening of the insulator gap in the electronic spectrum and the occurrence of the antiferromagnetic ordering. The occurrence of the long-range magnetic order caused by the condensation of local magnetic excitons is found.

The mechanism of the excitonic phase formation in the spin crossover area can be explained in Fig. 8. For the HS and LS ground states,

$$\langle -1 | X_A^{s,-} | -1 \rangle = \langle -1 | s \rangle = 0, \quad \langle s | X_A^{s,-} | s \rangle = 0.$$

In the excitonic phase the ground state is given by a linear superposition of the singlet and triplet with $\sigma = -1$ wave functions; see Eq. (24). That is why

$$\Delta_A^- = (v \langle -1 |_A + u \langle s |_A | X_A^{s,-} | u | s \rangle_A + v | -1 \rangle_A) = uv. \quad (25)$$

The exciton condensation in strongly correlated systems has been debated a lot in the literature (see, for example, [5,8–14]). The present theoretical studies for the excitonic-insulating phases have direct implications for the candidate materials of the excitonic-insulating state. The most relevant material is a series of the perovskite cobalt oxides $R_{1-x}A_x\text{CoO}_3$ and their family, in which the localized orbital picture works well. The low-temperature insulating phase in $\text{Pr}_{0.5}\text{Ca}_{0.5}\text{CoO}_3$, where any experimental indications for the magnetic and charge orders are not observed until now, is one of the possible candidates of excitonic-insulating phases [13,35–37].

For systems with a spin crossover, in which the ground state is LS and the HS state is separated from the ground state by spin gap ε_S , of particular interest are studies in strong magnetic fields [38–42], since the presence of the spin gap leads to the term crossing at $B = B_c$ (the magnetic-field-induced spin crossover). As an example, we presented the recently discovered magnetic transition in LaCoO_3 in a strong magnetic field [39], which can be related to the condensation of magnetic excitons [43,44]. The investigated model can be used to describe the extraordinary behavior of LaCoO_3 [39] and $(\text{Pr}_{1-y}\text{Y}_y)_{0.7}\text{Ca}_{0.3}\text{CoO}_3$ [45] in strong magnetic fields. The ground state in LaCoO_3 is confirmed experimentally as a nonmagnetic LS band insulator. We expect that LaCoO_3 is located near the phase boundary between the LS and HS-AFM-Ex phases in Fig. 3. This fact implies that the LS state in LaCoO_3 is possibly changed into the HS-AFM-Ex phase by changing an energy balance between the Hund coupling and the crystalline field splitting. Applying the magnetic field and/or expanding the lattice constant by chemical substitution or by utilizing the thin-film technique on a substrate are the plausible routes.

The other class of experiments with spin crossover is a high-pressure study of the Mott-Hubbard insulators; see the review paper [46]. Nevertheless for particular transition metal oxides a more complicated multiband analysis is required;

see for example the discussion of the spin crossover and its effect on the Mott-Hubbard transition in [30]. Here we restrict ourselves by a simplified two-band model that allows study of the excitonic condensation in the vicinity of spin crossover. But the method for calculating the electronic band structure in the different phases that we proposed can be used to calculate the electronic structure of real, strongly correlated systems at different external conditions (temperature, pressure, magnetic field, etc.).

One of the differences between our work and previous ones is the calculation of the temperature dependence of the main thermodynamic characteristics and phase diagrams of magnetization and excitonic order parameter in the coordinates of the crystal field–temperature. We consider that these calculations are more justified from the experimental point of view, since the intra-ionic parameters of the Coulomb interaction are practically independent of external conditions, and complement the existing understanding of physics of the excitonic phase in strongly correlated systems.

ACKNOWLEDGMENT

The authors thank the Russian Scientific Foundation for financial support under Grant No. 18-12-00022.

-
- [1] N. F. Mott, The transition to the metallic state, *Philos. Mag.* **6**, 287 (1961).
 - [2] R. Knox, *Theory of Excitons*, Supplement 5 to *Solid State Physics*, edited by F. Seitz and D. Turnbull (Academic Press, New York, 1963).
 - [3] L. V. Keldysh and Y. V. Kopaev, Possible instability of semimetallic state toward Coulomb interaction, *Sov. Phys. Solid State* **6**, 2219 (1965).
 - [4] J. D. Cloizeaux, Exciton instability and crystallographic anomalies in semiconductors, *J. Phys. Chem. Solids* **26**, 259 (1965).
 - [5] J. Kuneš, Excitonic condensation in systems of strongly correlated electrons, *J. Phys.: Condens. Matter* **27**, 333201 (2015).
 - [6] M. Blume, V. J. Emery, and R. B. Griffiths, Ising model for the λ transition and phase separation in He^3 - He^4 mixtures, *Phys. Rev. A* **4**, 1071 (1971).
 - [7] S. Sachdev and R. N. Bhatt, Bond-operator representation of quantum spins: Mean-field theory of frustrated quantum Heisenberg antiferromagnets, *Phys. Rev. B* **41**, 9323 (1990).
 - [8] J. Nasu, T. Watanabe, M. Naka, and S. Ishihara, Phase diagram and collective excitations in an excitonic insulator from an orbital physics viewpoint, *Phys. Rev. B* **93**, 205136 (2016).
 - [9] P. Werner and A. J. Millis, High-Spin to Low-Spin and Orbital Polarization Transitions in Multiorbital Mott Systems, *Phys. Rev. Lett.* **99**, 126405 (2007).
 - [10] R. Suzuki, T. Watanabe, and S. Ishihara, Spin-state transition and phase separation in a multiorbital Hubbard model, *Phys. Rev. B* **80**, 054410 (2009).
 - [11] L. Balents, Excitonic order at strong coupling: Pseudospin, doping, and ferromagnetism, *Phys. Rev. B* **62**, 2346 (2000).
 - [12] T. Kaneko and Y. Ohta, Roles of Hund's rule coupling in excitonic density-wave states, *Phys. Rev. B* **90**, 245144 (2014).
 - [13] J. Kunes and P. Augustinsky, Excitonic instability at the spin-state transition in the two-band Hubbard model, *Phys. Rev. B* **89**, 115134 (2014).
 - [14] J. Kuneš, Phase diagram of exciton condensate in doped two-band Hubbard model, *Phys. Rev. B* **90**, 235140 (2014).
 - [15] V. I. Kuz'min, Y. S. Orlov, A. E. Zarubin, T. M. Ovchinnikova, and S. G. Ovchinnikov, Magnetism in spin crossover systems: Short-range order and effects beyond the Heisenberg model, *Phys. Rev. B* **100**, 144429 (2019).
 - [16] J. Hubbard, Electron correlations in narrow energy bands. IV. The atomic representation, *Proc. R. Soc. London A* **285**, 542 (1965).
 - [17] J. Kanamori, Electron correlation and ferromagnetism of transition metals, *Prog. Theor. Phys.* **30**, 275 (1963).
 - [18] J. Hubbard, Electron correlations in narrow energy bands. II. The degenerate band case, *Proc. R. Soc. London A* **277**, 237 (1964).
 - [19] R. Zaitsev, Diagram technique and gas approximation in the Hubbard model, *Sov. Phys. JETP* **43**, 574 (1976).
 - [20] K. A. Chao, J. Spalek, and A. M. Oles, Kinetic exchange interaction in a narrow s -band, *J. Phys. C* **10**, L271 (1977).
 - [21] V. A. Gavrichkov, S. I. Polukeev, and S. G. Ovchinnikov, Contribution from optically excited many-electron states to the superexchange interaction in Mott-Hubbard insulators, *Phys. Rev. B* **95**, 144424 (2017).
 - [22] V. Val'kov and S. Ovchinnikov, Hubbard operators and spin-wave theory of Heisenberg magnets with arbitrary spin, *Theor. Math. Phys.* **50**, 306 (1982).
 - [23] M. J. R. Hoch, S. Nellutla, J. van Tol, E. S. Choi, J. Lu, H. Zheng, and J. F. Mitchell, Diamagnetic to paramagnetic transition in LaCoO_3 , *Phys. Rev. B* **79**, 214421 (2009).

- [24] B. A. Volkov, Y. V. Kopaev, and A. I. Rusinov, Theory of “excitonic” ferromagnetism, *Sov. Phys. JETP* **41**, 952 (1975).
- [25] S. G. Ovchinnikov and V. V. Val’kov, *Hubbard Operators in the Theory of Strongly Correlated Electrons* (Imperial College Press, London, 2004).
- [26] S. G. Ovchinnikov, V. A. Gavrichkov, M. M. Korshunov, and E. I. Shneyder, LDA+GTB method for band structure calculations in the strongly correlated materials, in *Strongly Correlated Systems: Theoretical Methods*, Springer Series in Solid-State Sciences, edited by A. Avella and F. Mancini (Springer, Berlin, 2012), Vol. 171, pp. 143–172.
- [27] Y. S. Orlov, S. V. Nikolaev, and V. A. Dudnikov, Effect of crystal field on the electronic structure of the two-band Hubbard model with spin crossover, *J. Exp. Theor. Phys.* **130**, 699 (2020).
- [28] J. Zaanen, G. A. Sawatzky, and J. W. Allen, Band Gaps and Electronic Structure of Transition-Metal Compounds, *Phys. Rev. Lett.* **55**, 418 (1985).
- [29] Y. Tanabe and S. Sugano, On the absorption spectra of complex ions. I, *J. Phys. Soc. Jpn.* **9**, 753 (1954).
- [30] S. G. Ovchinnikov, Analysis of the sequence of insulator-metal phase transitions at high pressure in systems with spin crossovers, *J. Exp. Theor. Phys.* **116**, 123 (2013).
- [31] S. G. Ovchinnikov, Effect of spin crossovers on the Mott-Hubbard transition at high pressures, *J. Exp. Theor. Phys.* **107**, 140 (2008).
- [32] A. G. Gavriluk, I. A. Trojan, S. G. Ovchinnikov, I. S. Lyubutin, and V. A. Sarkisyan, The mechanism of suppression of strong electron correlations in FeBO_3 at high pressures, *J. Exp. Theor. Phys.* **99**, 566 (2004).
- [33] I. S. Lyubutin, S. G. Ovchinnikov, A. G. Gavriluk, and V. V. Struzhkin, Spin-crossover-induced Mott transition and the other scenarios of metallization in $3d^n$ metal compounds, *Phys. Rev. B* **79**, 085125 (2009).
- [34] V. A. Gavrichkov, Y. S. Orlov, T. M. Ovchinnikova, and S. G. Ovchinnikov, Mechanisms of the insulator-metal transition and spin crossover in CoO at high pressure, *JETP Lett.* **112**, 241 (2020).
- [35] S. Tsubouchi, T. Kyômen, M. Itoh, P. Ganguly, M. Oguni, Y. Shimojo, Y. Morii, and Y. Ishii, Simultaneous metal-insulator and spin-state transitions in $\text{Pr}_{0.5}\text{Ca}_{0.5}\text{CoO}_3$, *Phys. Rev. B* **66**, 052418 (2002).
- [36] T. Fujita, T. Miyashita, Y. Yasui, Y. Kobayashi, M. Sato, E. Nishibori, M. Sakata, Y. Shimojo, N. Igawa, Y. Ishii, K. Kakurai, T. Adachi, Y. Ohishi, and M. Takata, Transport and magnetic studies on the spin state transition of $\text{Pr}_{1-x}\text{Ca}_x\text{CoO}_3$ up to high pressure, *J. Phys. Soc. Jpn.* **73**, 1987 (2004).
- [37] J. Kuneš and P. Augustinský, Excitonic condensation of strongly correlated electrons: The case of $\text{Pr}_{0.5}\text{Ca}_{0.5}\text{CoO}_3$, *Phys. Rev. B* **90**, 235112 (2014).
- [38] K. Sato, A. Matsuo, K. Kindo, Y. Kobayashi, and K. Asai, Field induced spin-state transition in LaCoO_3 , *J. Phys. Soc. Jpn.* **78**, 093702 (2009).
- [39] A. Ikeda, T. Nomura, Y. H. Matsuda, A. Matsuo, K. Kindo, and K. Sato, Spin state ordering of strongly correlating LaCoO_3 induced at ultrahigh magnetic fields, *Phys. Rev. B* **93**, 220401(R) (2016).
- [40] V. V. Platonov, Y. B. Kudasov, M. P. Monakhov, and O. M. Tatsenko, Magnetically induced phase transitions in LaCoO_3 in fields of up to 500 T, *Phys. Solid State* **54**, 279 (2012).
- [41] M. M. Altarawneh, G.-W. Chern, N. Harrison, C. D. Batista, A. Uchida, M. Jaime, D. G. Rickel, S. A. Crooker, C. H. Mielke, J. B. Betts, J. F. Mitchell, and M. J. R. Hoch, Cascade of Magnetic Field Induced Spin Transitions in LaCoO_3 , *Phys. Rev. Lett.* **109**, 037201 (2012).
- [42] M. Rotter, Z.-S. Wang, A. T. Boothroyd, D. Prabhakaran, A. Tanaka, and M. Doerr, Mechanism of spin crossover in LaCoO_3 resolved by shape magnetostriction in pulsed magnetic fields, *Sci. Rep.* **4**, 7003 (2014).
- [43] A. Sotnikov and J. Kuneš, Field-induced exciton condensation in LaCoO_3 , *Sci. Rep.* **6**, 30510 (2016).
- [44] T. Tatsuno, E. Mizoguchi, J. Nasu, M. Naka, and S. Ishihara, Magnetic field effects in a correlated electron system with spin-state degree of freedom: Implications for an excitonic insulator, *J. Phys. Soc. Jpn.* **85**, 083706 (2016).
- [45] A. Ikeda, S. Lee, T. T. Terashima, Y. H. Matsuda, M. Tokunaga, and T. Naito, Magnetic-field-induced spin crossover of Y-doped $\text{Pr}_{0.7}\text{Ca}_{0.3}\text{CoO}_3$, *Phys. Rev. B* **94**, 115129 (2016).
- [46] I. S. Lyubutin and A. G. Gavriluk, Research on phase transformations in 3d-metal oxides at high and ultrahigh pressure: State of the art, *Phys. Usp.* **52**, 989 (2009).